AGU PUBLICATIONS

JGR

Journal of Geophysical Research: Biogeosciences

RESEARCH ARTICLE
10.1002/2015JG003054

Key Points:
- Multiscale, nonlinear, asynchronous dynamics of methane flux are analyzed
- Traditional linear correlation misses important lagged, cross-scale dynamics
- Short-term water table and plant dynamics influence seasonal methane flux

Supporting Information:
- Supporting Information S1

Correspondence to:
C. Sturtevant,
cove.sturtevant@gmail.com

Citation:
Sturtevant, C., B. L. Ruddell, S. H. Knox, J. Verfaillie, J. H. Matthes, P. Y. Oikawa, and D. Baldocchi (2016), Identifying scale-emergent, nonlinear, asynchronous processes of wetland methane exchange, *J. Geophys. Res. Biogeosci.*, *121*, doi:10.1002/2015JG003054.

Received 14 MAY 2015
Accepted 16 DEC 2015
Accepted article online 20 DEC 2015

Identifying scale-emergent, nonlinear, asynchronous processes of wetland methane exchange

Cove Sturtevant[1], Benjamin L. Ruddell[2], Sara Helen Knox[1], Joseph Verfaillie[1], Jaclyn Hatala Matthes[3], Patricia Y. Oikawa[1], and Dennis Baldocchi[1]

[1]Ecosystem Sciences Division, Department of Environmental Science, Policy, and Management, University of California, Berkeley, California, USA, [2]Fulton School of Engineering, Arizona State University, Tempe, Arizona, USA, [3]Department of Geography, Dartmouth College, Hanover, New Hampshire, USA

Abstract Methane (CH_4) exchange in wetlands is complex, involving nonlinear asynchronous processes across diverse time scales. These processes and time scales are poorly characterized at the whole-ecosystem level, yet are crucial for accurate representation of CH_4 exchange in process models. We used a combination of wavelet analysis and information theory to analyze interactions between whole-ecosystem CH_4 flux and biophysical drivers in two restored wetlands of Northern California from hourly to seasonal time scales, explicitly questioning assumptions of linear, synchronous, single-scale analysis. Although seasonal variability in CH_4 exchange was dominantly and synchronously controlled by soil temperature, water table fluctuations, and plant activity were important synchronous and asynchronous controls at shorter time scales that propagated to the seasonal scale. Intermittent, subsurface water table decline promoted short-term pulses of methane emission but ultimately decreased seasonal CH_4 emission through subsequent inhibition after rewetting. Methane efflux also shared information with evapotranspiration from hourly to multiday scales and the strength and timing of hourly and diel interactions suggested the strong importance of internal gas transport in regulating short-term emission. Traditional linear correlation analysis was generally capable of capturing the major diel and seasonal relationships, but mesoscale, asynchronous interactions and nonlinear, cross-scale effects were unresolved yet important for a deeper understanding of methane flux dynamics. We encourage wider use of these methods to aid interpretation and modeling of long-term continuous measurements of trace gas and energy exchange.

1. Introduction

The most challenging aspect of understanding ecosystem functioning is accounting for overlapping, asynchronous, nonlinear processes. This is especially daunting when interpreting long-term continuous measurements of wetland methane (CH_4) exchange where scale-specific, nonlinear, and asynchronous processes can dominate [*Kettunen et al.*, 1996; *Moore and Dalva*, 1993; *Reid et al.*, 2013; *Updegraff et al.*, 2001]. For example, methane emission in response to water table fluctuation can be nonlinear and lagged by up to 10 days [*Moore and Dalva*, 1993] while also responding to seasonal variation in soil temperature [*Turetsky et al.*, 2014]. Diurnal carbon assimilation is known to stimulate CH_4 production in rice, but with a 1–1.5 h time lag [*Hatala et al.*, 2012a]. Adequately representing these dynamics in process models is important, especially in the context of emerging carbon markets where predicted methane emissions will reduce the net greenhouse gas benefit (and financial incentive) of wetland creation for carbon storage [*Mack et al.*, 2012]. However, our ability to adequately model whole-ecosystem wetland methane emissions is rudimentary [*Bridgham et al.*, 2013], in part due to poorly resolved dynamics over a wide range of conditions at the whole-ecosystem level [*Turetsky et al.*, 2014]. As more long-term eddy covariance studies of wetland methane exchange become available, this is increasingly becoming a problem not of data availability but of our ability to interpret it.

Traditional statistical analysis often ignores scale and assumes linearity and/or synchronicity, which outside of select experiments under controlled environmental conditions limits the characterization of important dynamics. These complexities call for addressing scale, nonlinearity, and asynchrony directly in analysis of biophysical flux time series with more tailored methods such as wavelet decomposition and information theory.

Wavelets have been recognized as a particularly powerful tool to address scale in geophysical and ecological analysis [*Cazelles et al.*, 2008; *Kumar and Foufoula-Georgiou*, 1997; *Torrence and Compo*, 1998], as wavelet decomposition characterizes both the time scale and location of patterns and perturbations in the data.

The temporal (or spatial) data series of a continuous environmental variable is the superposition of variation occurring at many different scales. Biophysical processes drive these patterns, and partitioning variability at different scales can help to isolate and characterize important processes. Wavelets have been successfully used to characterize the spatial scales of turbulent fluxes as well as the time scales of interaction between fluxes and biophysical drivers [*Ding et al*., 2013; *Fares et al*., 2013; *Katul et al*., 2001; *Katul and Parlange*, 1995; *Koebsch et al*., 2015; *Qin et al*., 2008; *Yoshida et al*., 2010]. Recent application of wavelet analysis to eddy covariance CH_4 flux time series has already expanded understanding of scale-wise wetland CH_4 dynamics, including control of the diel CH_4 flux pattern by carbon assimilation in rice [*Hatala et al*., 2012a] and the control of seasonal CH_4 emissions in a minerotrophic mire by air or water temperature depending on the position of the water table [*Koebsch et al*., 2015]. Finally, wavelet spectra have also been useful in evaluating physiological flux models to identify the time scales (and processes) of harmony and disharmony between predictions and observations [*Braswell et al*., 2005; *Dietze et al*., 2011; *Richardson et al*., 2007; *Stoy et al*., 2005].

One limitation of traditional spectral methods to identify flux processes is that they assume linearity. Thus, it is beneficial to combine wavelet analysis with tools well suited to handle nonlinear, and asynchronous effects. One such tool is information theory. Originating in the field of communication, Shannon entropy quantifies the probabilistic uncertainty (i.e., variability) of a process [*Shannon*, 1948]. Information content and Shannon entropy are the foundation for ecologically relevant determinants such as the well-known Akaike information criterion for model selection [*Akaike*, 1973], optimum spatial resolution of remote sensing imagery in ecological modeling or upscaling [*Stoy et al*., 2009a; *Stoy et al*., 2009b], and numerous measures of ecological complexity [*Parrott*, 2010]. Entropy metrics incorporating joint probabilities, such as mutual information and transfer entropy, quantify information overlap or flow between systems and indicate the dependency of one variable on another without assuming the analytical form or timing of the relationship. The robustness of information metrics to nonlinearity and asynchrony has already improved our understanding of the feedback network of processes influencing CO_2 and H_2O exchange across ecosystems [*Ruddell and Kumar*, 2009a, 2009b] and the sensitivity and dynamics of biosphere-atmosphere exchange to climate variability [*Kumar and Ruddell*, 2010; *Ruddell et al*., 2015]. Despite these benefits, combining wavelets and information theory to understand multiscale eco-atmosphere interactions is rare, and thus far has only been applied to terrestrial upland sites [*Brunsell and Anderson*, 2011; *Brunsell and Wilson*, 2013; *Brunsell et al*., 2008]. To our knowledge, multiscale information theory analysis has not yet been leveraged to interpret measurements of whole-ecosystem wetland methane exchange.

Here we address scale, nonlinearity, and asynchrony directly by using a combination of wavelet decomposition and information theory to analyze long-term, quasi-continuous, whole-ecosystem CH_4 flux time series from two restored wetlands in Northern California. By using wavelets to isolate the time scales of variation and information theory to identify biosphere-atmosphere interactions regardless of form or asynchrony, we systematically identified (1) the dominant biosphere-atmosphere flux processes and the time scales they act at, (2) their nonlinear and asynchronous characteristics, and (3) how they contributed to the strength and timing of biosphere-atmosphere exchange. We compare results to those derived from linear correlation analysis to evaluate what these methods can add to the traditional approach and contribute to modeling efforts. This analysis allows us to answer the question: What do we miss by assuming linearity and/or synchronicity and ignoring scale-specific interactions?

2. Methods

2.1. Study Sites

The study sites were in the Sacramento-San Joaquin Delta, a large inland river delta in Northern California, USA, experiencing a Mediterranean climate. Mean annual air temperature and precipitation are 15.0 ± 0.4 (SD)°C and 324.5 ± 118 mm, respectively (1998–2013; California Irrigation Management Information System, Twitchell Island station). The Delta region was drained for agricultural use beginning in the midnineteenth century [*Atwater and Belknap*, 1980; *Drexler et al*., 2007], and our measurements were conducted at two restored freshwater wetlands constructed on former agricultural sites and underlain by peat soils. They shared nearly identical meteorology and were dominated by similar *Scheonoplectus acutus* (tule) and *Typha* spp. (cattail) vegetation, with the plant active period extending approximately between May and October.

Table 1. Variable Descriptions

Symbol	Description	Unit
Q_p	photosynthetic photon flux density	$\mu mol\ m^{-2}\ s^{-1}$
T_a	air temperature	°C
T_w	water temperature, 10 cm above soil	°C
T_s	soil temperature, 32 cm depth	°C
D	saturation vapor pressure deficit	kPa
p_a	air pressure	kPa
H_w	height of water table above soil	cm
O	dissolved O_2 in the water column	$mg\ L^{-1}$
θ	wind direction	°N
$u*$	friction velocity	$m\ s^{-1}$
E	water vapor flux density	$mmol\ m^{-2}\ s^{-1}$
F_{CO2}	net CO_2 flux density	$\mu mol\ m^{-2}\ s^{-1}$
G	gross CO_2 assimilation	$\mu mol\ m^{-2}\ s^{-1}$
R	ecosystem CO_2 respiration	$\mu mol\ m^{-2}\ s^{-1}$
F_{CH4}	CH_4 flux density	$nmol\ m^{-2}\ s^{-1}$

The first wetland was Ameriflux site US-Tw1, a 0.028 km^2 wetland constructed in 1997 (site photos provided in Figure S7 in the supporting information), with flux measurements beginning in July 2012. Vegetation coverage was 100% in this "old" wetland over the entire measurement period, with a relatively greater proportion of *S. acutus*. The second wetland was Ameriflux site US-Myb, a 1.21 km^2 wetland constructed in 2010 approximately 12.5 km southwest of the old wetland. This "young" wetland was designed with areas of shallow and deep water to create a mosaic of open water and vegetation. Flux measurements at the young wetland began in December of 2010. Fractional vegetation coverage increased from $<$10% in 2010 to approximately 75% in 2015, with a relatively greater proportion of *Typha* spp. Both wetlands were enclosed (isolated from tidal influence), and the California Department of Water Resources pumped water in from the Delta system to maintain water levels, also making water levels insensitive to precipitation. Measurements of surface sediment in 2012 indicated similar belowground conditions between the wetlands, with slight acidity (pH ~ 6.3 at the old wetland, pH ~ 6.7 at the young wetland), similar soil carbon content (~20%), and high total Fe concentration (~9 mg Fe/g soil) (G. McNicol, unpublished data). Salinity (measured by conductivity) was low but was higher at the young wetland and increased fairly steadily in both wetlands over their respective measurement periods, from ~0.2 to 1.6 $mS\ cm^{-1}$ at the old wetland and from ~1 to 6 $mS\ cm^{-1}$ at the young wetland. For more information about the history of these sites, we refer the reader to *Matthes et al*. [2014], *Knox et al*. [2015], *Byrd et al*. [2014], and *Miller* [2011]. For seasonal dynamics (explained below), we analyzed the entire available record of flux measurements at each site: from July 2012 to July 2015 at the old wetland, and from December 2010 to July 2015 at the young wetland. For shorter-term flux dynamics we focused on the growing season of 2013.

2.2. Flux and Environmental Measurements

Biosphere-atmosphere exchange of CO_2 (F_{CO2}), CH_4 (F_{CH4}), and H_2O (E) were measured using the eddy covariance method [*Baldocchi et al*., 1988] and were accompanied by a suite of supporting environmental measurements (Table 1) as described in *Knox et al*. [2015]. Flux instrumentation and processing were identical between the sites. A sonic anemometer (Windmaster, Gill Instruments Ltd., Lymington, Hampshire, UK) measured high-frequency 3-D wind speed components and virtual temperature at 4.6 m and 3.7 m above the typical water surface in the old and young wetlands, respectively. Open-path infrared gas analyzers measured molar concentrations of CO_2, H_2O (LI-7500A, LI-COR Biosciences Inc., Lincoln, NE, USA) and CH_4 (LI-7700, LI-COR Biosciences Inc., Lincoln, NE, USA). Raw flux measurements were recorded at 10 Hz on an analyzer interface unit (LI-7550, LI-COR Biosciences Inc., Lincoln, NE, USA) and 30 min fluxes were calculated with in-house MATLAB software (v. 8.4, Mathworks, Inc., Natick, MA, USA) [*Detto et al*., 2010; *Hatala et al*., 2012b; *Knox et al*., 2015]. Supporting environmental measurements were recorded as 30 min averages on a data logger.

Quality control procedures [*Foken et al*., 2004] as described in *Knox et al*. [2015] retained original flux measurements for 37% (62–66%) in the old (young) wetlands. However, 2013 growing season (day of year (DOY) 130–300) data retention was much higher, 74% (85–90%) in the old (young) wetland. Because wavelet

decomposition requires special treatment of gaps, data gaps were filled prior to wavelet decomposition. We used an artificial neural network (ANN) approach [*Baldocchi et al*., 2015; *Knox et al*., 2015] in order to preserve the overall shape of the data patterns without assuming functional relationships between variables. F_{CO2} was gap-filled with two separate ANNs, one for daytime conditions, and one for nighttime. Gross CO_2 assimilation (G) and ecosystem respiration (R) were estimated by extrapolating the ANN trained for nighttime F_{CO2} to the entire day [*Baldocchi et al*., 2015]. Although the ANN approach does not assume functional relationships, the ANN gap-filling did not account for potential lagged interactions between variables. Thus, after wavelet decomposition (see below) original gaps were subsequently removed prior to information theory analysis in all but the seasonal time scale. We did not remove original gaps at the seasonal scale because gap lengths were small relative to this scale.

2.3. Linear Correlation Analysis

Bivariate linear correlation was performed on the average F_{CH4} diel pattern during the 2013 growing season (DOY 130–300) and on daily average gap-filled F_{CH4} over the full measurement periods. We chose these two methods for comparison because they continue to form the traditional analysis performed on eddy covariance and chamber measurements of F_{CH4} (for example, *Alberto et al*. [2014], *Hendriks et al*. [2010], *Strachan et al*. [2015], *Sun et al*. [2013], and *Turetsky et al*. [2014]). We note that more sophisticated statistical analysis is certainly in practice, such as the use of classification and regression trees [*Sachs et al*., 2008], though still typically employed on daily averaged data.

2.4. Wavelet-based Time Scale Decomposition

Time scales of variability in fluxes and environmental variables were decomposed using the maximal-overlap discrete wavelet transform (MODWT) [*Percival*, 1995]. We chose the MODWT over the traditional orthonormal discrete wavelet transform (ODWT) because MODWT retains the capability of multiresolution analysis while lacking the sensitivity of the ODWT wavelet coefficients to the starting position of the wavelet averaging window within the time series [*Cornish et al*., 2006]. At each scale j the MODWT applies a high-pass wavelet filter $\widetilde{h}_{j,l}$ and low-pass scaling filter $\widetilde{g}_{j,l}$ of length l to time series X to respectively yield wavelet coefficients $\widetilde{W}_{j,t}$ and scaling coefficients $\widetilde{V}_{j,t}$ for every point t in the time series [*Percival and Walden*, 2000]:

$$\widetilde{W}_{j,t} = \sum_{l=0}^{L_j-1} \widetilde{h}_{j,l} X'_{t-l \bmod 2N} \tag{1}$$

$$\widetilde{V}_{j,t} = \sum_{l=0}^{L_j-1} \widetilde{g}_{j,l} X'_{t-l \bmod 2N} \tag{2}$$

where $X' = X$ for $t = 0 \ldots N$ and $X' = X_{2N-1-t}$ for $t = N \ldots 2N\text{-}1$ represents the use of a reflected boundary condition [*Cornish et al*., 2006]. The $\widetilde{W}_{j,t}$ wavelet coefficients distinguish fluctuations in the time series of scale 2^{j-1} data points, while the $\widetilde{V}_{j,t}$ coefficients characterize the fluctuations at scale 2^j points and higher. Expressing equations (1) and (2) in matrix notation, $\widetilde{W}_j = \widetilde{\mathbf{W}}_j X$ and $\widetilde{\mathbf{V}}_j = \widetilde{\mathbf{V}}_j X$, where the nonbolded symbols are vectors the same length as the time series X and the bolded symbols $\widetilde{\mathbf{W}}_j$ and $\widetilde{\mathbf{V}}_j$ are matrices with rows containing circularly shifted versions of the upsampled and periodized filters $\widetilde{h}_{j,l}$ and $\widetilde{g}_{j,l}$, respectively [see *Percival and Walden*, 2000], the detail $\widetilde{D}_j$ and smooth $\widetilde{S}_j$ reconstructions of the time series at each scale are derived as:

$$\widetilde{D}_j = \widetilde{\mathbf{W}}_j^T \widetilde{W}_j \tag{3}$$

$$\widetilde{S}_j = \widetilde{\mathbf{V}}_j^T \widetilde{V}_j \tag{4}$$

so that the sum of the detail reconstructions $\widetilde{D}_j$ up to maximum scale J_0 and remaining smooth component of the time series $\widetilde{S}_{J_0}$ reconstruct the original signal:

$$X = \sum_{j=1}^{J_0} \widetilde{D}_j + \widetilde{S}_{J_0} \tag{5}$$

This is known as wavelet-based multiresolution analysis [*Mallat*, 1989]. The time series can be decomposed into the detail added from successively coarser to finer scales, and either summed or evaluated individually to analyze patterns at varying scales.

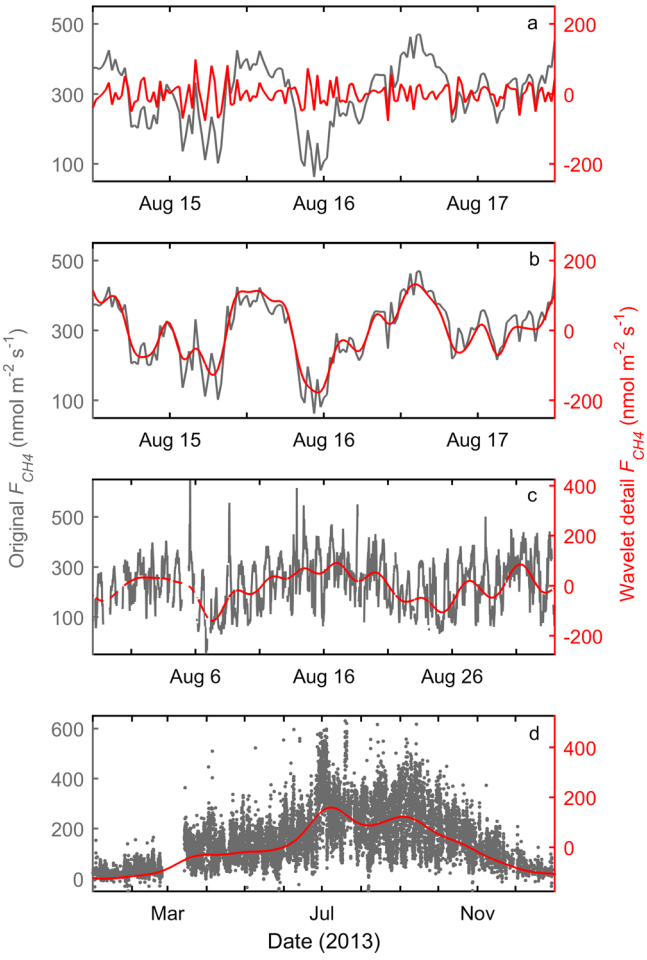

Figure 1. Example F_{CH4} variation isolated with wavelet decomposition at the (a) hourly, (b) diel, (c) multiday, and (d) seasonal time scales. Gray lines and points are original half-hourly measurements. The red line indicates the wavelet detail reconstruction.

In our analysis we used the Least Symmetric 8 (LA8) wavelet filter, as resultant wavelet coefficients are less correlated across time scales and contain less contamination from adjacent scales compared to the traditional Haar wavelet, while maintaining a relatively low number of coefficients influenced by boundary conditions [*Cornish et al.*, 2006].

We reconstructed the detail ($\widetilde{D}_j$) in the fluxes and environmental variables for dyadic scales 1 (2^1 measurements = 1 h) to 14 (2^{14} measurements = 341 days). Because patterns resulting from ecological processes naturally occur over a scale range rather than one specific scale, we summed the detail over adjacent scales to analyze four general time scales of variation: Scales 1 and 2 (1–2 h) form the "hourly" scale (Figure 1a), representing perturbations such as clouds passing overhead and turbulent scales up to the spectral gap. Scales 3–6 (4 h to 1.3 days) form the "diel" scale (Figure 1b), representing the day-night cycle in sunlight and temperature. Scales 7–10 (2.7–21.3 days) form the "multiday" scale (Figure 1c), identifying synoptic weather variability and variations in water table. Lastly, scales 11–14 (42.7–341 days) form the "seasonal" scale, representing the annual solar cycle and phenology (Figure 1d).

2.5. Characterizing Eco-atmosphere Interactions Using Information Theory

In information theory, mutual information [*Fraser and Swinney*, 1986], or I describes the average tendency for paired states of two variables (say, X and Y) to coexist. I_{XY} is computed using the marginal and joint probability distributions of X and Y, most commonly expressed in bits (base-2):

$$I_{XY} = \sum_{x_t}\sum_{y_t} p(x_t, y_t)\log_2\frac{p(x_t, y_t)}{p(x_t)p(y_t)} \tag{6}$$

where x_t and y_t are all the states that X and Y, respectively, can take. The "states" of continuous variables are delineated by binning the data (discussed below). I_{XY} can also be expressed, albeit less intuitively, in terms of the Shannon entropy [*Shannon*, 1948], H, which is a measure of uncertainty:

$$I_{XY} = H_X + H_Y - H_{XY} \tag{7}$$

$$H_X = -\sum_{x_t} p(x_t)\log_2 p(x_t) \tag{8}$$

$$H_Y = -\sum_{y_t} p(y_t)\log_2 p(y_t) \tag{9}$$

$$H_{XY} = -\sum_{x_t}\sum_{y_t} p(x_t, y_t)\log_2 p(x_t, y_t) \tag{10}$$

The relative mutual information $I^R_{XY} = I_{XY}/H_Y$ represents the proportion of bits needed to represent Y that are superfluous given the knowledge of X. In other words, it is a normalized measure of statistical dependence of Y on X, with higher values indicating greater dependence. We use this relative form of mutual information in presenting our results because it is the most intuitive, and use the term "interaction" to indicate the degree of mutual information, or nonindependence between X and Y.

The power of I_{XY} lies in the lack of parametric assumptions about the relationship between X and Y and is thus able to identify linear and nonlinear interactions alike. This utility is enhanced further by adding temporal directionality in I_{XY} [*Schreiber*, 2000]:

$$I_{XY}(\tau) = \sum_{x_{t-\tau}} \sum_{y_t} p(x_{t-\tau}, y_t) \log_2 \frac{p(x_{t-\tau}, y_t)}{p(x_{t-\tau}) p(y_t)} \tag{11}$$

In relative form:

$$I^R_{XY}(\tau) = \frac{\sum_{x_{t-\tau}} \sum_{y_t} p(x_{t-\tau}, y_t) \log_2 \frac{p(x_{t-\tau}, y_t)}{p(x_{t-\tau}) p(y_t)}}{-\sum_{y_t} p(y_t) \log_2 p(y_t)} \tag{12}$$

where τ represents a lead ($\tau < 0$) or lag ($\tau > 0$) in series Y relative to X (both being functions of time, t). We define a "synchronous" interaction as one in which the maximum I^R_{XY} is observed at zero time lag ($\tau = 0$), meaning that variations in Y have the strongest dependence on concurrent variations in X. An interaction is "asynchronous" when it is otherwise. Maximum I^R_{XY} at $\tau > 0$ means that variations in Y have a stronger dependence on previous variations in X. Conversely, maximum I^R_{XY} at $\tau < 0$ indicates that variations in Y lead variations in X. In this way, I is able to identify the statistical strength and asynchrony of complex eco-atmosphere interactions.

I does not distinguish between linear and nonlinear interactions. To make this distinction we also computed the linearized mutual information, also called linear redundancy, L [*Paluš*, 2008]:

$$L_{XY}(\tau) = -\frac{1}{2} \sum_{i=1}^{2} \log_2 [\sigma_i(\tau)] \tag{13}$$

where $\sigma_i(\tau)$ are the eigenvalues of the correlation matrix for $X_{t-\tau}$ and Y_t. Mutual information and linear redundancy are theoretically equivalent when X and Y have Gaussian distributions [*Paluš*, 2008].

2.6. Identifying Eco-atmosphere Interactions in a Multiresolution Framework

Data were first wavelet-decomposed into the hourly, diel, multiday, and seasonal time scales outlined above using the WMTSA Wavelet Toolkit in MATLAB [*Cornish et al*., 2003]. Then, the relative mutual information (I^R) between F_{CH4} and biophysical drivers was computed within each time scale as well as across time scales over a range of time lags (τ) using version 1.5 of the ProcessNetwork Software [*Ruddell et al*., 2008]. Maximum evaluated lags were limited to 1 day at the hourly scale, 2 days at the diel scale, 10 days at the multiday scale, and 100 days at the seasonal scale. For cross-scale interactions, evaluated lags corresponded to the larger of the two scales. We define "upscaling" as a significant interaction between biophysical variables at shorter time scales and F_{CH4} at longer time scales, whereas "downscaling" indicates a significant interaction between biophysical variables at longer time scales and F_{CH4} at shorter time scales. We define "scale-emergence" as significant interactions that become dominant at some scales but not others.

For the hourly to multiday scales the analysis was confined to the growing season of 2013 (DOY 130–300). We chose the growing season as the focus of our analysis at shorter time scales because it is the period when the fluxes and their variations are strongest and dynamical entropy highest [*Ruddell and Kumar*, 2009a]. In addition, the growing season of 2013 presented strong differences in water table variation between the old and young wetlands, which provided an excellent case study on the significance of differing water table dynamics on F_{CH4}. To avoid wavelet-induced border distortions at the hourly to multiday scales, we decomposed the entire available time series and then clipped the data to the appropriate period. We did not exclude boundary regions in the seasonal analysis, as the data were near-stationary at this scale, which minimizes boundary distortions [*Cornish et al*., 2006].

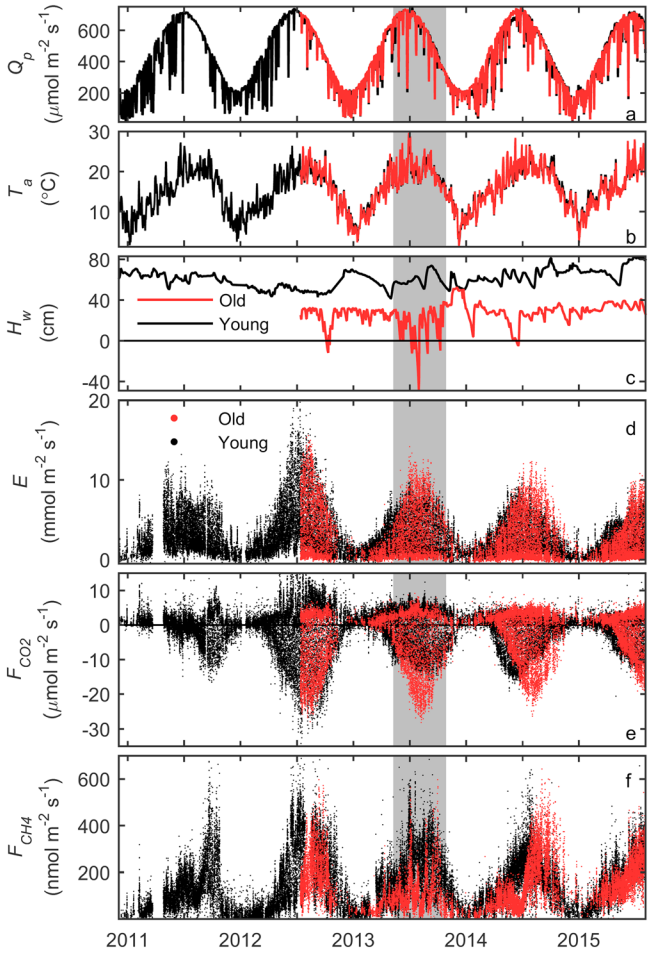

Figure 2. Daily average environmental conditions and half-hourly greenhouse gas fluxes in the old and young wetlands (see Table 1 for variable descriptions). The vertical shaded area delineates the growing season of 2013 used in the analysis from hourly to multiday scales.

To estimate the probabilities in equation (12), each variable was discretized into 10 fixed-interval histogram bins. This binning scheme was found to result in sufficient process resolution to identify complex interactions while minimizing bias due to finite sample sizes (see supporting information). To avoid outliers disrupting bin resolution, total bin range was determined by excluding the lowest and highest 1% of values, forcing the extreme points into the first and last bins, respectively. Table S1 in the supporting information presents the physical resolutions corresponding to this binning scheme.

Statistical significance at the 95% level was determined using a Monte Carlo approach with random walks (see supporting information), applying the same sequence of computational procedures as in the analysis. Additional tests on synthetic time series characterized the response of I^R with interaction strength (Figure S5) and the minimum resolvable lag (Figure S6). Very strong interactions at the hourly to multiday scales showed $I^R > 0.5$, and $I^R > 0.35$ at the seasonal scale. Moderate-strength interactions showed $I^R > 0.1$ at the hourly and diel scales, $I^R > 0.07$ at the multiday scale, and $I^R > 0.05$ at the seasonal scale. Lag errors were ~0 for $I^R > 0.04$ and $I^R > 0.05$ for the hourly and diel scales, respectively. At the multiday scale, lag error was ~0 for $I^R > 0.25$, increasing to ~1 day for $I^R < 0.1$. At the seasonal scale the lag error was < 4 days for $I^R > 0.2$.

3. Results

3.1. Environmental Conditions During the Study Period

Due to their proximity, meteorological conditions were very similar between the sites (Figures 2a and 2b). Photosynthetic flux density (Q_p) followed a strong seasonal pattern, with the time series punctuated by short periods of cloud cover (Figure 2a). Air (and soil) temperatures peaked later in the season than radiation (Figure 2b). The water table in the young wetland was consistently managed at a level that was always well above the surface with generally slow variation (Figure 2c). Conversely, the water table in the old wetland was a lower height above the soil surface and managed variably, falling sharply to or below the surface several times and especially throughout the 2013 growing season as a result of pump failure events.

3.2. Methane Fluxes and Time Scales of Variability

Methane fluxes exhibited strong variability in both wetlands (Figure 2f) over a range of time scales (Figure 3a). The seasonal time scale dominated F_{CH4} variability in both wetlands and was particularly pronounced in the young wetland, whereas the seasonal F_{CH4} variation in the old wetland was more balanced with diel variation. F_{CH4} variation at hourly and multiday scales was generally low, although multiday F_{CH4} variation in the old wetland was much stronger in 2013 (Figure 3b), which corresponded with multiple F_{CH4} peaks (Figure 2f)

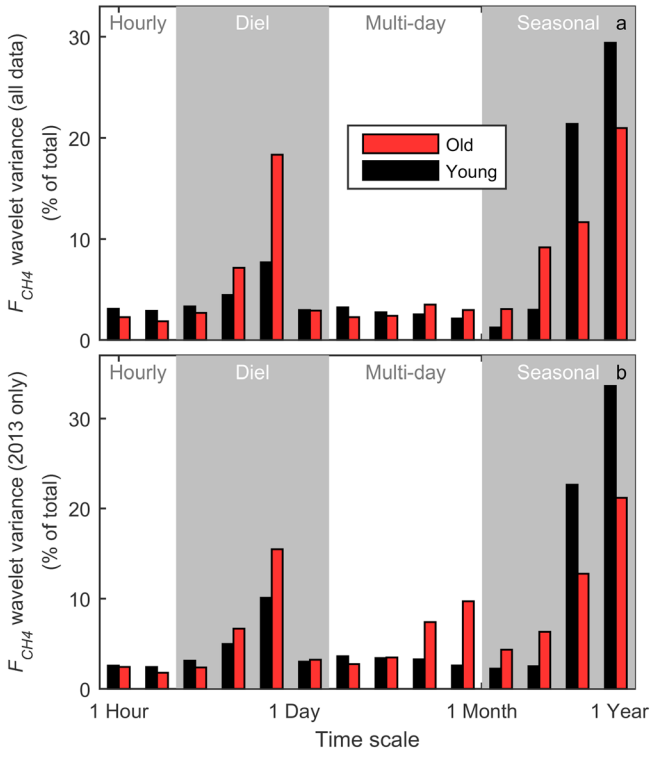

Figure 3. Variance of F_{CH4} wavelet coefficients at each time scale, as a percentage of the total variance, for (a) all analyzed data and (b) 2013 only. Alternating gray-white shading highlights the four time scale groupings used for analysis.

and a highly variable water table (Figure 2c) during the 2013 growing season. Excluding 2011 (the first year after restoration), annual budgets of F_{CH4} in the young wetland were quite stable, averaging 50 g C m^{-2} yr^{-1} with an absolute range of only 3.9 g C m^{-2} yr^{-1} from 2012 to 2014. In contrast, annual F_{CH4} emission at the old wetland for the two full years of measurements differed by 14 g C m^{-2} yr^{-1} (26 ± 2 g C m^{-2} yr^{-1} in 2013 and 40 ± 3 g C m^{-2} yr^{-1} in 2014).

3.3. Linear Correlation Analysis

The diel average pattern of F_{CH4} was most strongly correlated with Q_p, E, F_{CO2}, and G in the old wetland (Table 2). The young wetland shared a strong correlation with E but otherwise showed stronger correlations with air temperature (T_a), vapor pressure deficit (D), and R. These correlations were evident in the shape of the diel patterns (Figure 4), where F_{CH4}, E, and F_{CO2} all peaked near noon in the old wetland, while in the young wetland F_{CO2} peaked near noon but F_{CH4}, E, and T_a peaked later in the afternoon (along with D and R, not shown).

Analysis of daily average F_{CH4} showed the strongest (positive) correlations with soil and water temperatures at both sites (Table 2), although correlations were generally weaker in the old wetland. F_{CH4} in both wetlands also showed strong positive relationships with E and the partitioned F_{CO2} components G and R, although correlations were again weaker at the old site.

3.4. Multiscale Interactions Between F_{CH4} and Biophysical Variables

Figures 5 and 6 show how the relative mutual information (I^R) between F_{CH4} and biophysical variables changed from hourly to seasonal time scales in each the old wetland (Figure 5) and young wetland (Figure 6). These figures indicate the most significant eco-atmosphere interactions at each time scale (indicated by the length of the bars) and whether a lead or lag was involved in the process (indicated by colored extensions to the bars). The bolded diagonal subplots in each figure show same-scale interactions, whereas the off-diagonal subplots show interactions between temporal scales (cross-scale interactions), where variability in biophysical variables at the scale of each row shared information with F_{CH4} variability at the scale of each column. For example, Figures 5l and 6l show how variability in biophysical variables at the multiday scale shared information with F_{CH4} variability at the seasonal scale. We note that each subplot in Figures 5 and 6 is another way to visualize a dynamical process network [*Ruddell and Kumar*, 2009b]. For the interested reader, we provide analogous Figures 5 and 6 for F_{CO2} in the supporting information (Figures S8 and S9), although we interpret only the results for F_{CH4} here.

3.4.1. Influence of Plant Activity on F_{CH4}

Although there were significant cross-scale interactions, the strongest interactions between F_{CH4} and biophysical variables occurred within the same temporal scale in both wetlands (diagonal plots in Figures 5 and 6). At the diel scale (Figures 5f and 6f) the results were similar to those of the linear correlation analysis, with the strongest shared information between E and F_{CH4} in both wetlands. In the old wetland, diel variation in F_{CH4} led E by 1 h whereas in the young wetland F_{CH4} lagged E by 0.5 h. This analysis of diel variability is slightly

Table 2. Bivariate Correlations Between the F_{CH4} and Biophysical Variables

	Diel Average F_{CH4} Pattern (2013 Growing Season)		Daily Average F_{CH4} (All Data)	
Variable	Old	New	Old	New
Q_p	0.96	0.83	0.50	0.71
T_a	0.77	0.98	0.60	0.80
T_w	0.41	−0.02	0.67	0.81
T_s	−0.78	0.34	0.66	0.81
D	0.74	0.98	0.41	0.62
p_a	0.56	0.06	−0.52	−0.60
H_w	0.01	0.07	−0.11	−0.03
O	−0.83	0.56	0.06	−0.07
θ	0.74	0.53	0.15	0.37
$u*$	0.68	0.42	0.45	0.71
E	0.95	0.95	0.63	0.77
F_{CO2}	−0.94	−0.79	−0.57	−0.59
G	−0.94	−0.84	−0.64	−0.79
R	0.46	0.97	0.66	0.73

different from the correlation analysis of the diel pattern in that I^R reflects not only similarity in the shape of the diel pattern but also in the magnitude of diel variability. Thus, although the lags differed between the wetlands, they both shared similarity in day-to-day differences in the diel magnitude of E and F_{CH4}. The different synchronies between diel F_{CH4} and other variables reflects the different timings of the diel F_{CH4} patterns between the wetlands (Figure 4), F_{CH4} peaking with light and F_{CO2} near noon at the old wetland versus later in the afternoon with T_a in the young wetland. Interestingly, information on the diel variability in Q_p, E, F_{CO2}, and G scaled up to seasonal variability in F_{CH4} (Figures 5h and 6h), indicating that diel variation in photosynthesis-related variables was related to the shape, strength, and timing of the seasonal F_{CH4} pattern.

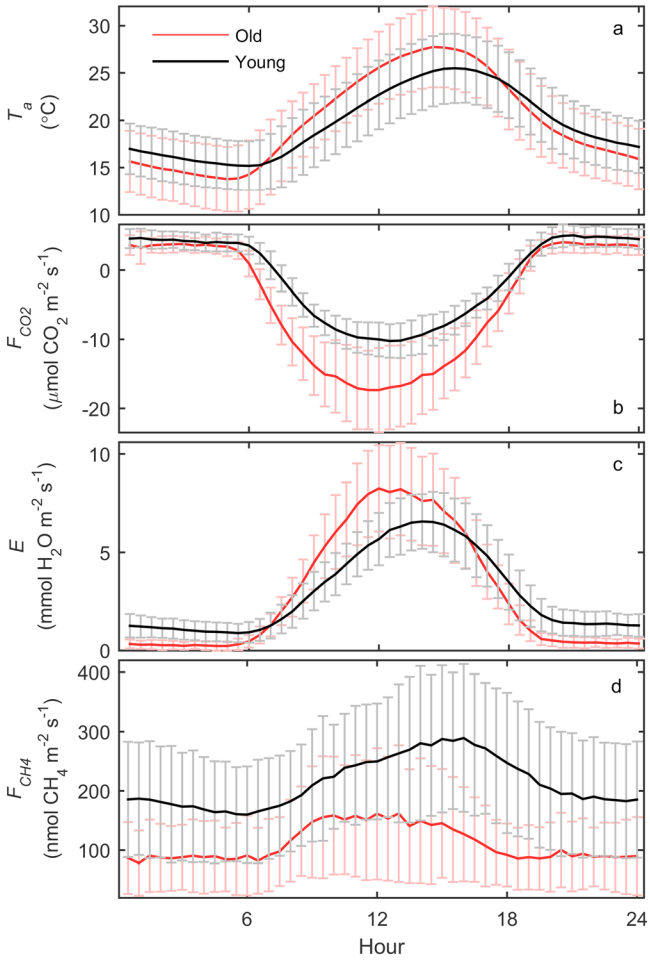

Figure 4. Diel average patterns of (a) T_a, (b) F_{CO2}, (c) E, and (d) F_{CH4} during the 2013 growing season. Error bars represent the standard deviation of the mean.

The dominant interaction between F_{CH4} and E at both sites was also present in the hourly scale (Figures 5a and 6a). However, this was synchronous and to the exclusion of the other strong interactions observed at the diel scale. The exception to this was the additionally dominant I^R between F_{CH4} and wind direction (θ) in the young wetland, which was also observed at the diel and multiday scales (Figures 6a, 6f, and 6k) yet was unidentified in the linear correlation analysis of the diel average pattern and daily averages (Table 2). This indicated that spatial variability was an important aspect of subseasonal F_{CH4} variation in the young wetland as the flux footprint shifted with θ over various patches of vegetation and open water.

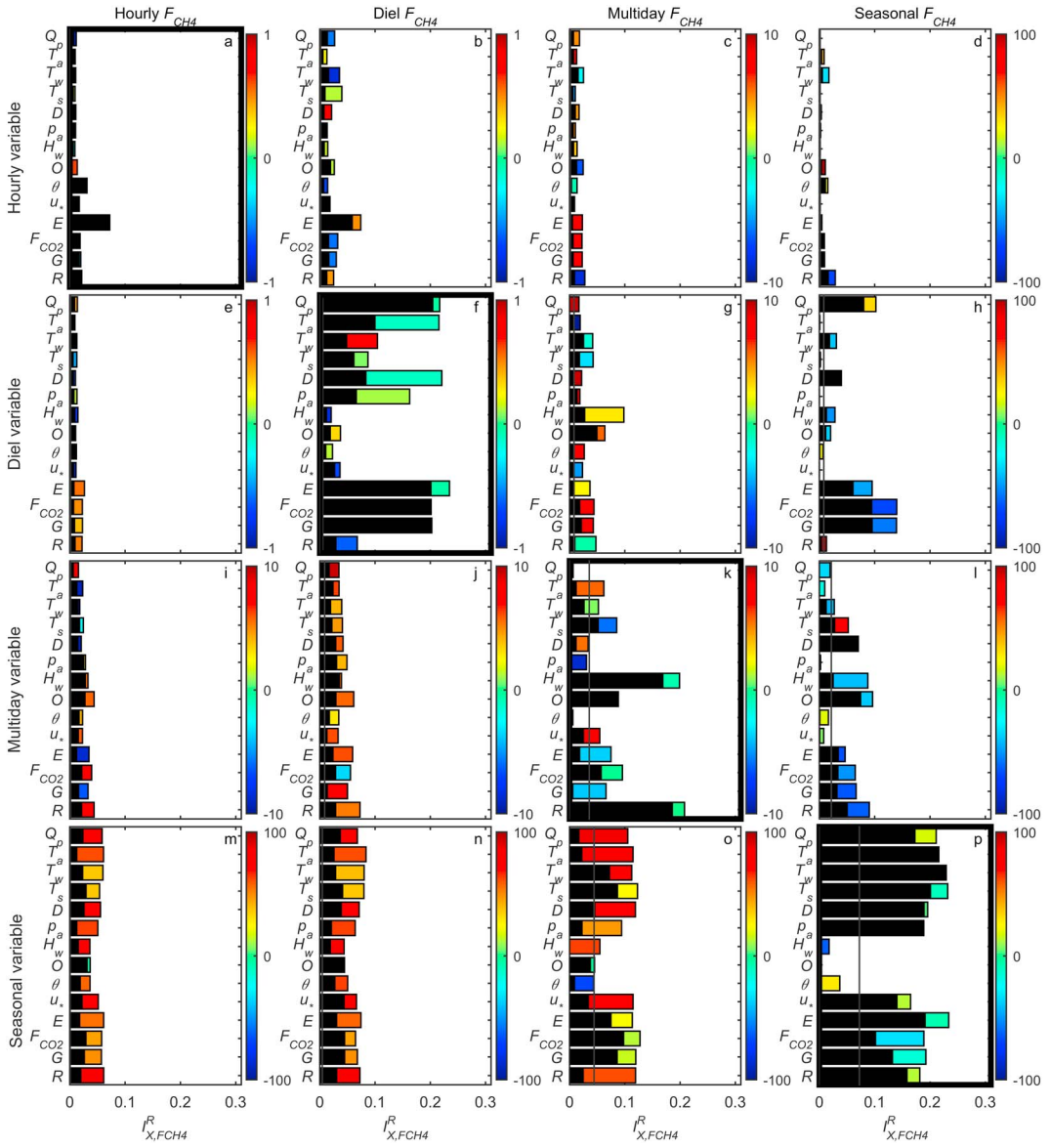

Figure 5. Relative mutual information ($I^R_{X,FCH4}$) between F_{CH4} and biophysical variables (X represents each variable on the y axis) from hourly to seasonal time scales in the old wetland. The bolded diagonal subplots show same-scale interactions, and the off-diagonal subplots show cross-scale interactions, where variability in biophysical variables at the scale of each row shared information with F_{CH4} variability at the scale of each column (upper diagonal subplots show upscaled information; lower diagonal subplots show downscaled information). The length of the black portion of each bar indicates I^R at zero time lag, and a colored extension indicates the maximum I^R and the lead or lag at which it occurred (indicated by color, color bar units in days). Negative lag (blue) indicates that variability in F_{CH4} led variability in the biophysical variable. Positive lag (yellow-red) indicates F_{CH4} lagged the biophysical variable. The vertical gray line in each subplot is the 95% significance threshold.

3.4.2. Influence of Water Table Fluctuation on F_{CH4}

At the multiday scale the dominant interactions changed considerably at the old wetland (Figure 5k), with significant I^R between F_{CH4} and water table height (H_w) as well as R. Examination of $I^R_{Hw,FCH4}$ with lag (Figure 7a) showed a primary interaction where variation in F_{CH4} slightly led variation in H_w ($\tau = -16$ h), but also a secondary interaction where F_{CH4} lagged H_w. The wavelet detail reconstruction for these variables (Figure 7b) showed that large CH_4 pulses (up to 200 nmol m^{-2} s^{-1}) typically occurred with minimums in water table but preceded the minimum for large water table declines. The lower strength but synchronous interaction between F_{CH4} and dissolved oxygen (O) at this scale (Figures 5k and 7a) hints

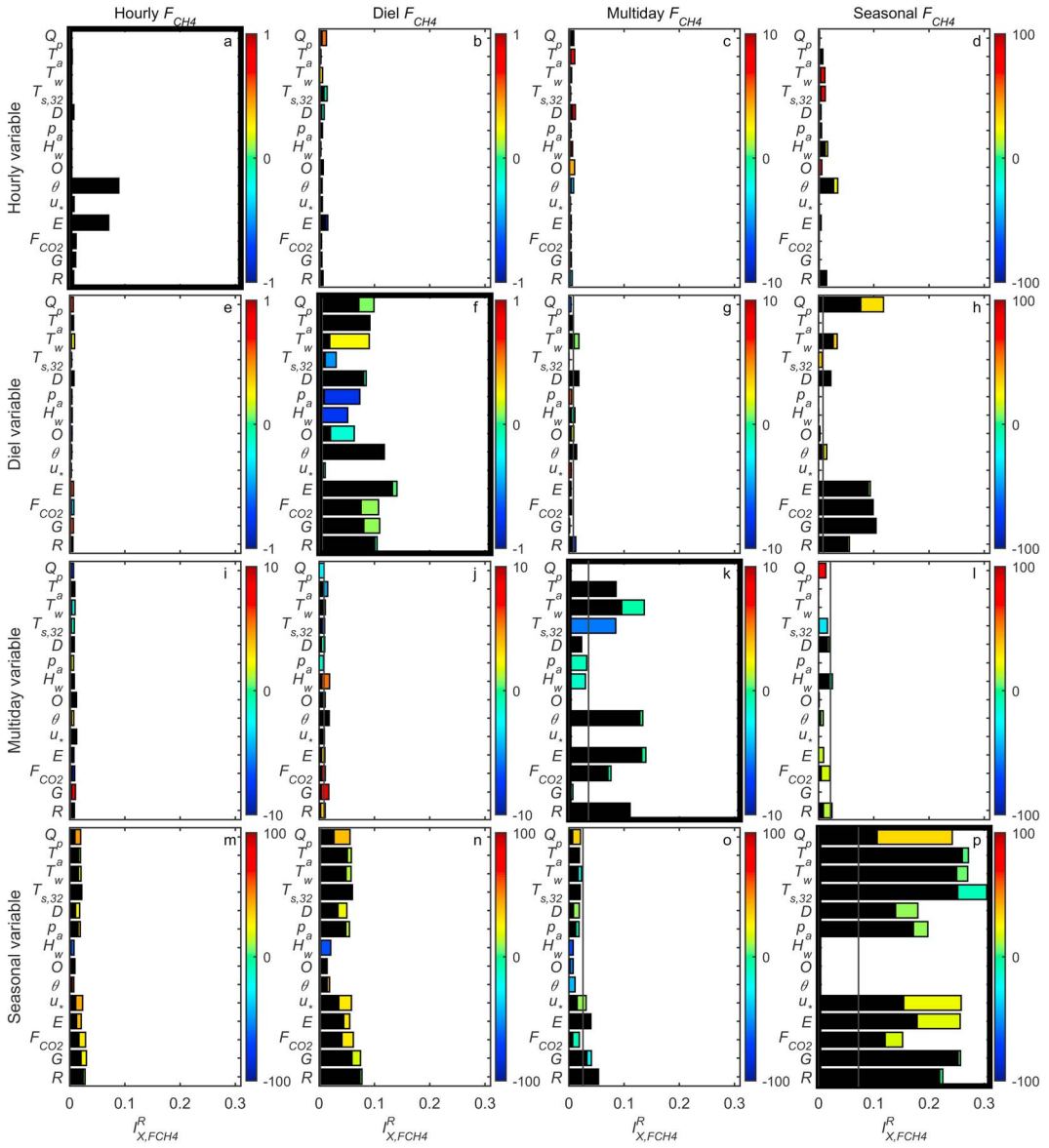

Figure 6. Relative mutual information ($I^R_{X,FCH4}$) between F_{CH4} and biophysical variables (X represents each variable on the y axis) from hourly to seasonal time scales in the young wetland. For explanation see Figure 5.

to the reason: peak F_{CH4} occurred as the water table crossed the soil surface and before the minimum in water table. Lower $I^R_{O,FCH4}$ reflects the fact that that water table declines that did not cross the soil surface (O remaining relatively constant) still corresponded with increased F_{CH4} (Figure 7b), thus diminishing the average interaction between O and F_{CH4} at this scale. This complexity is also highlighted in the differential magnitude of F_{CH4} pulses for similar declines in water table (Figure 7b) and in the statistically significant information on H_w variation included in F_{CH4} up to a lag of 10 days (Figure 7a). This lagged secondary interaction was a result of often lower F_{CH4} after a subsequent rise in water table than before the drop (Figure 7b).

Information on diel and multiday H_w and O variability in the old wetland also scaled up to multiday (Figure 5g) and seasonal (Figure 5l) F_{CH4} variability, respectively. Diel H_w contributed information to multiday F_{CH4} variation at a peak lag of 3 days, which corresponded well with the lagged portion of $I^R_{Hw,FCH4}$ observed in the same-scale multiday interaction (Figure 5a). Diel H_w variation in the old wetland represented the sharp increases in water table after managers reset the pumps, thus capturing the lagged decrease in F_{CH4} after H_w

returned to normal, higher levels. Upscaled multiday H_w and O variation led the F_{CH4} pattern by ~40 days (Figures 5l and 7c). This corresponded with peak growing season F_{CH4} emissions that occurred prior to periods of highly variable water table, and the lower magnitude of the F_{CH4} seasonal pattern during 2013 when water table variation was greatest (Figure 7d). The shift to the stronger I^R between O and F_{CH4} in this multiday to seasonal cross-scale interaction indicates that water table declines that fell below the surface were most responsible for this pattern.

3.4.3. Influence of Temperature on Seasonal Scale F_{CH4}

At the seasonal scale, the strongest I^R between F_{CH4} and biophysical drivers in both wetlands was with air (T_a), water (T_w), and 32 cm soil temperatures (T_s), where all lagged the seasonal increase in light availability (Q_p) (Figures 5p and 6p). The short lead in the seasonal F_{CH4} pattern from that of T_s likely reflected the strongest link to soil temperature at a depth nearer the soil surface than at 32 cm. Notably, seasonal F_{CH4} variability in the old wetland shared less information and was not synchronous with G and R, compared to stronger and synchronous interactions in the young wetland, perhaps reflecting the disruptive influence of multi day H_w and O on the F_{CH4} seasonal pattern in the old wetland.

Seasonal variability in biophysical variables scaled down to variability in F_{CH4} at shorter time scales (Figures 5m–5o and 6m–6o) that matched the general pattern of interactions observed in the same-scale seasonal interactions (Figures 5p and 6p). This indicated that F_{CH4} variability from hourly to multiday scales experienced seasonality along with the seasonal pattern of biophysical drivers. These downscale interactions tended to be stronger in the old wetland and generally corresponded with the greater partitioning of F_{CH4} variability to shorter scales at that site (Figure 3).

3.4.4. Multiscale F_{CH4} Analysis With a Linear Estimator

Comparison of the mutual information results presented in Figures 5 and 6 with those of the linear redundancy (Figures S10 and S11) revealed that all of the same-scale interactions (diagonal subplots in Figures 5 and 6) were resolvable with the linear estimator. However, none of the cross-scale interactions were identified. This was because a linear process results in a proportional response that by definition only occurs at the same time scale. Most importantly, the linear estimator missed the upscaling of shorter-scale plant activity and water table variability to the seasonal pattern of F_{CH4} (compare subplots h and l of Figures 5 and 6 with those of Figures S10 and S11, respectively).

4. Discussion

This is the first study to address scale, asynchrony, and nonlinearity directly with a combination of wavelet decomposition and information theory to analyze time series of wetland CH_4 exchange. Addressing scale separated the dominant seasonal F_{CH4} control by soil temperature so that additionally important dynamics associated with plant activity and water table variation could be resolved. Scale-emergent asynchrony between the diel patterns of CO_2 and CH_4 exchange in the young wetland points to the mechanism of internal gas transport in linking CH_4 exchange with transpiration (detailed below). Isolating the control of water table on CH_4 exchange across scales revealed both synchronous and asynchronous effects which opposed each other, promoting immediate CH_4 release while subsequently inhibiting it. Finally, addressing nonlinearity (and scale) revealed that information on diel plant activity and multiday water table variations propagated to the seasonal scale to modulate cumulative emissions. Identification of these cross-scale interactions was by definition not possible with a linear estimator and serves as strong motivation to use nonlinear estimators in multiscale analysis.

4.1. Dynamics of CH_4 Exchange

Owing to the greatest proportion of F_{CH4} variability at the seasonal scale in both wetlands and the strong I^R between F_{CH4} and T_s at this scale, this study agrees with many others across a range of wetland ecosystems that have indicated soil temperature as the greatest control over wetland CH_4 emission (for example, *Chu et al.* [2014], *Ding and Cai* [2007], *Long et al.* [2010], *Sachs et al.* [2008], *Sun et al.* [2013]. *Turetsky et al.* [2014], and *Wille et al.* [2008]). This result was expected given that the majority of previous studies used correlation analysis of daily average fluxes to analyze seasonal variability. However, the identification of upscaled information from diel and multiday scales to the seasonal scale identified how plant activity and water table dynamics at shorter time scales also moderate seasonal CH_4 emission.

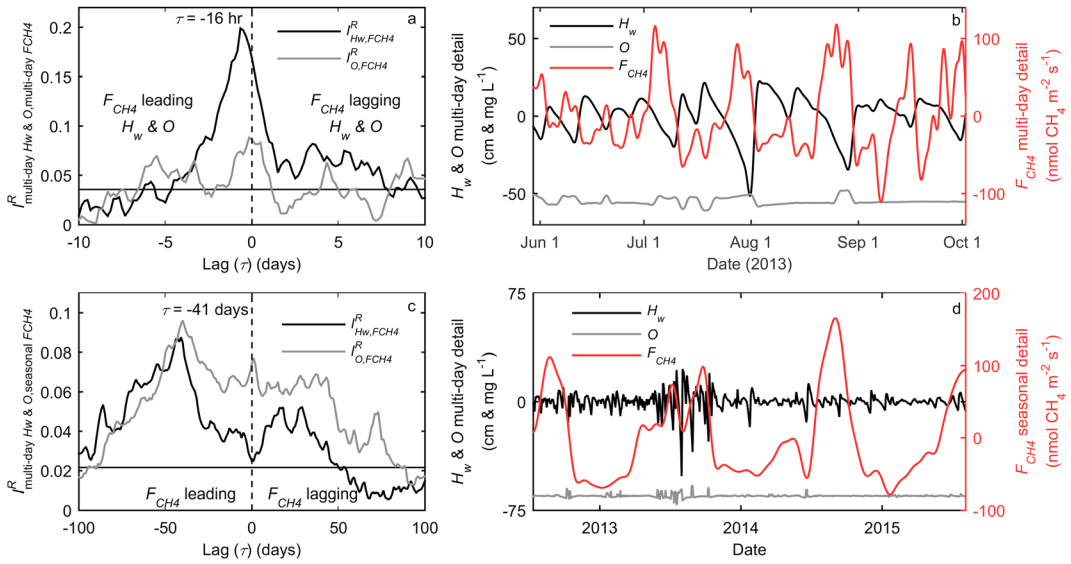

Figure 7. Relative mutual information (I^R) (a and c) between F_{CH4} and water table (H_w) or dissolved oxygen (O) in the old wetland as a function of lag and (b and d) subsets of the wavelet detail reconstructions of F_{CH4}, H_w, and O. Figures 7a and 7b show same-scale multiday interactions, whereas Figures 7c and 7d show cross-scale multiday to seasonal interactions. Note that the mean is removed in wavelet detail reconstructions; thus, the y axes in Figures 7b and 7d are relative rather than absolute, and O in Figures 7b and 7d is offset for clarity. The horizontal line in Figures 7a and 7c denotes the 95% statistical significance level, and the lag (τ) of maximum I^R is included on the plot if not equal to zero.

4.1.1. Influence of Plant Activity on F_{CH4}

Evapotranspiration (E) was consistently and dominantly linked to F_{CH4} variability at hourly and diel scales in both wetlands and additionally at the multiday scale in the young wetland (i.e., in the absence of strong water table variation). At short time scales, the interaction with E likely represents transport of CH_4 through aerenchyma [*Garnet et al.*, 2005; *Miller*, 2011; *Morrissey et al.*, 1993], and this variability in E and carbon assimilation (G) was upscaled to influence seasonal F_{CH4} by representing the strength of plant activity and likely also increased labile carbon supply [*Hatala et al.*, 2012a; *Minoda and Kimura*, 1994; *Whiting and Chanton*, 1993].

The combination of wavelet decomposition and information theory revealed the dominance of gas transport as the driving mechanism for short-term variability in CH_4 flux. Although most studies agree that plant activity largely controls short-term (diel) patterns of wetland F_{CH4}, it is difficult to separate whether the strength of internal gas transport, stomatal conductance, or stimulation of methane production by recent carbon assimilation is the most direct mechanism [*Hatala et al.*, 2012a; *Hendriks et al.*, 2010; *Koebsch et al.*, 2015; *Morin et al.*, 2014; *Van der Nat et al.*, 1998; *Whiting and Chanton*, 1996]. Our analysis showed the synchronous link between E and F_{CH4} in the absence of corresponding links to G and Q_p at the hourly scale, indicating that internal gas transport, not recent photosynthate or stomatal conductance (represented by Q_p) controls the shortest-scale perturbations of F_{CH4}. This was further supported by comparing diel scale F_{CH4} patterns between the young and old wetlands, dominated by different species of emergent vegetation with contrasting gas exchange traits. The old wetland had a higher proportion of *S. acutus*, which uses diffusion to transport oxygen to roots [*Van der Nat et al.*, 1998]. Diffusive transport is associated with greatest CH_4 emission during peak light availability when stomatal aperture is largest [*Van der Nat et al.*, 1998], and this was the observed pattern in the old wetland. The young wetland had a greater proportion of *Typha* spp., which uses pressurized ventilation generated by a difference between internal and external humidity to force air down to roots which then exits through older, broken leaves [*Brix et al.*, 1992; *Chanton et al.*, 1993; *Grosse et al.*, 1996; *Stengel*, 1993]. Maximum internal gas flow rates in *Typha* spp. therefore occur later in the day with increased vapor pressure deficit (D) [*Brix et al.*, 1992; *Sorrell and Brix*, 2003], while stomatal conductance remains synchronous with light availability [*Whiting and Chanton*, 1996]. This matches the shift in the diel peaks of E and F_{CH4} observed in the young wetland toward the afternoon when D was highest. We note that the shift in E toward the afternoon in the young wetland was largely unrelated to the patchy open water at that site, as portable tower measurements in a densely vegetated portion of the wetland during 2014 showed the same

afternoon shift in E (Figure S12). Disentangling the effects of gas transport, photosynthetic carbon, and stomatal conductance on F_{CH4} is challenging and often addressed using costly tracers and isotopic techniques in laboratory environments. Wavelet decomposition and information theory are a valuable post hoc tool that can inform process modeling of the influence of plant activity and vegetation dynamics on CH_4 production and CH_4 transport.

4.1.2. Water Table Influence on Short- and Long-term Patterns of CH_4 Exchange

The strong water table variation in the old wetland during 2013 shifted CH_4 flux variance toward the time scales that water table varied (Figure 3) and contributed upscaled information to multiday and seasonal patterns (Figures 5g and 5l), demonstrating the important role of water table in modulating CH_4 emission at multiple time scales. Similar CH_4 pulses during water table drawdown have been noted by others [*Hatala et al*., 2012b; *Moore and Dalva*, 1993; *Windsor et al*., 1992]. The complex interactions identified in the old wetland (Figure 7) are consistent with the release of stored CH_4 as hydrostatic pressure decreased, with peak release occurring as the water table crossed the soil surface. Differential magnitudes of CH_4 pulses therefore depend on the rate of production and the current pool. The prolonged reduction in CH_4 emission upon water table rise could result from a period of replenishment of the soil CH_4 pool or the recharge of alternative electron acceptors (such as the large soil pool of Fe in both wetlands) during unsaturated conditions, causing a slow return to higher methane production potentials [*Kettunen et al*., 1999; *Moore and Dalva*, 1993]. Our analysis suggests the latter given that H_w and O variation at the multiday scale contributed information to seasonal F_{CH4} variability and that cumulative CH_4 emission in 2013 (when there were several drainage events) was lower than that of 2014 in which the water table was more stable. Intermittent drainage has been linked to overall lower CH_4 emissions in rice [*Alberto et al*., 2014; *Wassmann et al*., 2000; *Yagi et al*., 1996], as well as in temperate wetland chamber measurements [*Altor and Mitsch*, 2006, 2008], but has thus far not been reported in temperate marshes at the whole-ecosystem level.

Similar to other studies of wetland methane exchange in which the water table remains above the surface [*Hargreaves et al*., 2001; *Song et al*., 2011 1243; *Strachan et al*., 2015], CH_4 emission in the young wetland was not linked to water table variation at any scale, and a test of our analysis to the growing season of other years in the old wetland with less water table variation revealed much weaker H_w-F_{CH4} interactions. This highlights the limitation of observational studies to detect controls that do not vary, and the need for long-term continuous measurements of whole-ecosystem CH_4 exchange.

The asynchronous and cross-scale control of F_{CH4} variability by water table was not identified in the bivariate linear correlation analysis, and the linearized multiscale analysis was unable to capture the influence of shorter-scale water table variation on seasonal CH_4 emission. As proof of concept that this type of analysis can guide modeling efforts, incorporation of the lagged reduction in F_{CH4} after rewetting identified by this analysis into a F_{CH4} process model was key for good performance (Oikawa et al., Farming carbon instead of corn: A biogeochemical model for carbon market-funded wetland restoration, submitted to *Global Change Biology*, 2015). Thus, while this analysis does not provide a predictive model it provides the timing and scale-dependent variance information for guiding modeling efforts as well as the capability to evaluate how well models represent cross-scale, asynchronous, and nonlinear processes observed in the data.

4.2. Limitations

Two limitations highlight ways in which the application of information theory in a multiresolution framework can be improved. First, we did not explicitly account for partial or interactive effects among drivers. Although separating the time scales of variation was successful in isolating and therefore identifying dominant processes with mutual information, we acknowledge the work of *Sharma and Mehrotra* [2014] in developing partial information metrics, which may enable characterization of multiple drivers competing for dominance at the same time scale. In a conditional linear causal analysis, *Detto et al*. [2013] showed that interactions which appear direct and significant in bivariate analysis can actually be indirect when conditional relationships are accounted for. This is an important area of advancement for nonlinear estimators. The second improvement addresses causation in a nonlinear multiresolution framework. Mutual information quantifies information overlap between two variables, which is more akin to correlation. Assigning causation in environmental time series using Granger causality (a linear estimator) is fairly well developed [for example, *Detto et al*., 2012; *Hatala et al*., 2012a; *Molini et al*., 2010] and involves identifying relationships in which the

driver is able to predict future observations of the response variable better than the response can predict itself. One nonparametric information theory metric that implies causation is transfer entropy, which quantifies information flow rather than simply overlap [*Schreiber*, 2000] and reduces to Granger causality for vector autoregressive processes [*Barnett et al.*, 2009]. We chose mutual information over transfer entropy in our analysis due to its lower data requirements [*Ruddell and Kumar*, 2009b] and more intuitive statistical interpretation. In addition, we note that asynchronous mutual information at negative lag (response precedes driver) was useful in characterizing the timing of F_{CH4} pulses during drainage events. Since causality analysis assumes that variability in drivers precedes variability in the response, the timing of this effect would remain unresolved. However, testing the application of transfer entropy in a multiresolution framework is a logical next step.

5. Conclusion

Applying information theory in a wavelet-based multiresolution framework provided a systematic approach to address scale, asynchrony, and nonlinearity directly to provide a rich understanding of the controls and timing of biosphere-atmosphere flux dynamics needed for process modeling. Results from two case studies of hourly to seasonal methane flux variability in Northern California restored wetlands revealed important cross-scale, nonlinear, and asynchronous interactions that were not well resolved in traditional linear correlation analysis. Although seasonal variability in CH_4 exchange was dominantly and synchronously controlled by soil temperature, water table fluctuations and plant activity were important controls at shorter time scales that upscaled to modulate seasonal CH_4 emissions. Evapotranspiration, as driven by stomatal conductance and photosynthesis, most likely represented the strength of internal gas transport. It was responsible for hourly to multiday CH_4 flux variability in one wetland and hourly to diel variability in the other. Water table fluctuations in the latter wetland overrode the link between methane flux and evapotranspiration at the multiday scale, where subsurface drops in water table induced strong short-term CH_4 pulses, though ultimately reduced annual CH_4 emission via subsequent inhibition of CH_4 flux after rewetting. Methods that intrinsically account for scale, asynchrony, and nonlinearity deserve wider use in interpreting long-term continuous measurements of trace gas and energy exchange.

Acknowledgments

Data from US-Myb and US-Tw1 used in this study are freely available from Ameriflux (http://ameriflux.lbl.gov/). The ProcessNetwork software can be downloaded from the MATLAB Central File Exchange (http://www.mathworks.com/matlabcentral/fileexchange/41515-processnetwork-version-1-5-software). We thank Bryan Brock and the California Department of Water Resources for project funding (contract 4600008849). Additional funding was provided by the United States Department of Agriculture (NIFA grant 2011-67003-30371), the United States Department of Energy (AmeriFlux contract 7079856), and the National Science Foundation (grant EF-1241960). We thank Matteo Detto and another anonymous reviewer for helpful comments to improve the manuscript.

References

Akaike, H. (1973), Information theory and an extension of the maximum likelihood principle, in *Second International Symposium on Information Theory*, edited by B. N. Petrov and F. Csaki, pp. 267–281, Akademiai Kiado, Budapest.

Alberto, M. C. R., R. Wassmann, R. J. Buresh, J. R. Quilty, T. Q. Correa, J. M. Sandro, and C. A. R. Centeno (2014), Measuring methane flux from irrigated rice fields by eddy covariance method using open-path gas analyzer, *Field Crops Res.*, *160*, 12–21, doi:10.1016/j.fcr.2014.02.008.

Altor, A. E., and W. J. Mitsch (2006), Methane flux from created riparian marshes: Relationship to intermittent versus continuous inundation and emergent macrophytes, *Ecol. Eng.*, *28*(3), 224–234, doi:10.1016/j.ecoleng.2006.06.006.

Altor, A. E., and W. J. Mitsch (2008), Pulsing hydrology, methane emissions and carbon dioxide fluxes in created marshes: A 2-year ecosystem study, *Wetlands*, *28*(2), 423–438, doi:10.1672/07-98.1.

Atwater, B. F., and D. F. Belknap (1980), Tidal-wetland deposits of the Sacramento-San Joaquin Delta, California, paper presented at Pacific Coast Paleogeography Symposium.

Baldocchi, D. D., B. B. Hicks, and T. P. Meyers (1988), Measuring biosphere-atmosphere exchanges of biologically related gases with micrometeorological methods, *Ecology*, *69*(5), 1331–1340.

Baldocchi, D., C. Sturtevant, and FLUXNET Contributors (2015), Does day and night sampling reduce spurious correlation between canopy photosynthesis and ecosystem respiration?, *Agric. For. Meteorol.*, *207*, 117–126, doi:10.1016/j.agrformet.2015.03.010.

Barnett, L., A. B. Barrett, and A. K. Seth (2009), Granger causality and transfer entropy are equivalent for Gaussian variables, *Phys. Rev. Lett.*, *103*(23238701).

Braswell, B. H., W. J. Sacks, E. Linder, and D. S. Schimel (2005), Estimating diurnal to annual ecosystem parameters by synthesis of a carbon flux model with eddy covariance net ecosystem exchange observations, *Global Change Biol.*, *11*(2), 335–355, doi:10.1111/j.1365-2486.2005.00897.x.

Bridgham, S. D., H. Cadillo-Quiroz, J. K. Keller, and Q. Zhuang (2013), Methane emissions from wetlands: Biogeochemical, microbial, and modeling perspectives from local to global scales, *Global Change Biol.*, *19*(5), 1325–1346, doi:10.1111/gcb.12131.

Brix, H., B. K. Sorrell, and P. T. Orr (1992), Internal pressurization and convective gas-flow in some emergent fresh-water macrophytes, *Limnol. Oceanogr.*, *37*(7), 1420–1433.

Brunsell, N. A., and C. J. Wilson (2013), Multiscale interactions between water and carbon fluxes and environmental variables in a Central U.S. grassland, *Entropy*, *15*(4), 1324–1341, doi:10.3390/e15041324.

Brunsell, N. A., and M. C. Anderson (2011), Characterizing the multi-scale spatial structure of remotely sensed evapotranspiration with information theory, *Biogeosciences*, *8*(8), 2269–2280, doi:10.5194/bg-8-2269-2011.

Brunsell, N. A., J. M. Ham, and C. E. Owensby (2008), Assessing the multi-resolution information content of remotely sensed variables and elevation for evapotranspiration in a tall-grass prairie environment, *Remote Sens. Environ.*, *112*(6), 2977–2987, doi:10.1016/j.rse.2008.02.002.

Byrd, K. B., J. L. O'Connell, S. Di Tommaso, and M. Kelly (2014), Evaluation of sensor types and environmental controls on mapping biomass of coastal marsh emergent vegetation, *Remote Sens. Environ.*, *149*, 166–180, doi:10.1016/j.rse.2014.04.003.

Cazelles, B., M. Chavez, D. Berteaux, F. Ménard, J. Vik, S. Jenouvrier, and N. Stenseth (2008), Wavelet analysis of ecological time series, *Oecologia*, *156*(2), 287–304, doi:10.1007/s00442-008-0993-2.

Chanton, J. P., G. J. Whiting, J. D. Happell, and G. Gerard (1993), Contrasting rates and diurnal patterns of methane emission from emergent aquatic macrophytes, *Aquat. Bot.*, *46*(2), 111–128, doi:10.1016/0304-3770(93)90040-4.

Chu, H., J. Chen, J. F. Gottgens, Z. Ouyang, R. John, K. Czajkowski, and R. Becker (2014), Net ecosystem methane and carbon dioxide exchanges in a Lake Erie coastal marsh and a nearby cropland, *J. Geophys. Res. Biogeosci.*, *119*, 722–740, doi:10.1002/2013JG002520.

Cornish, C. R., D. B. Percival, and C. S. Bretherton (2003), The WMTSA Wavelet Toolkit for data analysis in the geosciences, *Eos Trans. AGU, 84*(46), Fall Meet. Suppl., Abstract NG11A-0173.

Cornish, C., C. Bretherton, and D. Percival (2006), Maximal overlap wavelet statistical analysis with application to atmospheric turbulence, *Boundary Layer Meteorol.*, *119*(2), 339–374, doi:10.1007/s10546-005-9011-y.

Detto, M., D. Baldocchi, and G. G. Katul (2010), Scaling properties of biologically active scalar concentration fluctuations in the atmospheric surface layer over a managed peatland, *Boundary Layer Meteorol.*, *136*(3), 407–430, doi:10.1007/s10546-010-9514-z.

Detto, M., A. Molini, G. Katul, P. Stoy, S. Palmroth, and D. Baldocchi (2012), Causality and persistence in ecological systems: A nonparametric spectral Granger causality approach, *Am. Natl.*, *179*(4), 524–535.

Detto, M., G. Bohrer, J. G. Nietz, K. D. Maurer, C. S. Vogel, C. M. Gough, and P. S. Curtis (2013), Multivariate conditional Granger causality analysis for lagged response of soil respiration in a temperate forest, *Entropy*, *15*(10), 4266–4284, doi:10.3390/e15104266.

Dietze, M. C., et al. (2011), Characterizing the performance of ecosystem models across time scales: A spectral analysis of the North American Carbon Program site-level synthesis, *J. Geophys. Res.*, *116*, G04029, doi:10.1029/2011JG001661.

Ding, R. S., S. Z. Kang, R. Vargas, Y. Q. Zhang, and X. M. Hao (2013), Multiscale spectral analysis of temporal variability in evapotranspiration over irrigated cropland in an arid region, *Agric. Water Manage.*, *130*, 79–89, doi:10.1016/j.agwat.2013.08.019.

Ding, W. X., and Z. C. Cai (2007), Methane emission from natural wetlands in China: Summary of years 1995–2004 studies, *Pedosphere*, *17*(4), 475–486, doi:10.1016/s1002-0160(07)60057-5.

Drexler, J. Z., C. S. de Fontaine, and D. L. Knifong (2007), Age determination of the remaining peat in the Sacramento-San Joaquin Delta, California, USA, *Rep. 2007–1303*, U.S. Geol. Surv., Sacramento, Calif.

Fares, S., R. Vargas, M. Detto, A. H. Goldstein, J. Karlik, E. Paoletti, and M. Vitale (2013), Tropospheric ozone reduces carbon assimilation in trees: Estimates from analysis of continuous flux measurements, *Global Change Biol.*, *19*(8), 2427–2443, doi:10.1111/gcb.12222.

Foken, T., M. Gockede, M. Mauder, L. Mahrt, B. Amiro, and W. Munger (2004), Post-field data quality control, in *Handbook of Micrometeorology: A Guide for Surface Flux Measurement and Analysis*, edited by X. Lee, W. J. Massman, and B. E. Law, pp. 181–208, Kluwer Acad., Dordrecht, Netherlands.

Fraser, A. M., and H. L. Swinney (1986), Independent coordinates for strange attractors from mutual information, *Phys. Rev. A*, *33*(2), 1134–1140.

Garnet, K. N., J. P. Megonigal, C. Litchfield, and G. E. Taylor (2005), Physiological control of leaf methane emission from wetland plants, *Aquat. Bot.*, *81*(2), 141–155, doi:10.1016/j.aquabot.2004.10.003.

Grosse, W., J. Armstrong, and W. Armstrong (1996), A history of pressurised gas-flow studies in plants, *Aquat. Bot.*, *54*(2–3), 87–100, doi:10.1016/0304-3770(96)01037-6.

Hargreaves, K. J., D. Fowler, C. E. R. Pitcairn, and M. Aurela (2001), Annual methane emission from Finnish mires estimated from eddy covariance campaign measurements, *Theor. Appl. Climatol.*, *70*(1–4), 203–213.

Hatala, J. A., M. Detto, and D. D. Baldocchi (2012a), Gross ecosystem photosynthesis causes a diurnal pattern in methane emission from rice, *Geophys. Res. Lett.*, *39*, L06409, doi:10.1029/2012GL051303.

Hatala, J. A., M. Detto, O. Sonnentag, S. J. Deverel, J. Verfaillie, and D. D. Baldocchi (2012b), Greenhouse gas (CO_2, CH_4, H_2O) fluxes from drained and flooded agricultural peatlands in the Sacramento-San Joaquin Delta, *Agric. Ecosyst. Environ.*, *150*, 1–18, doi:10.1016/j.agee.2012.01.009.

Hendriks, D. M. D., J. van Huissteden, and A. J. Dolman (2010), Multi-technique assessment of spatial and temporal variability of methane fluxes in a peat meadow, *Agric. For. Meteorol.*, *150*(6), 757–774, doi:10.1016/j.agrformet.2009.06.017.

Katul, G. G., and M. B. Parlange (1995), Analysis of land surface heat fluxes using the orthonormal wavelet approach, *Water Resour. Res.*, *31*(11), 2743–2749, doi:10.1029/95WR00003.

Katul, G., C.-T. Lai, K. Schäfer, B. Vidakovic, J. Albertson, D. Ellsworth, and R. Oren (2001), Multiscale analysis of vegetation surface fluxes: from seconds to years, *Adv. Water Resour.*, *24*(9–10), 1119–1132, doi:10.1016/S0309-1708(01)00029-X.

Kettunen, A., V. Kaitala, J. Alm, J. Silvola, H. Nykanen, and P. J. Martikainen (1996), Cross-correlation analysis of the dynamics of methane emissions from a boreal peatland, *Global Biogeochem. Cycles*, *10*(3), 457–471, doi:10.1029/96GB01609.

Kettunen, A., V. Kaitala, A. Lehtinen, A. Lohila, J. Alm, J. Silvola, and P. J. Martikainen (1999), Methane production and oxidation potentials in relation to water table fluctuations in two boreal mires, *Soil Biol. Biochem.*, *31*(12), 1741–1749, doi:10.1016/s0038-0717(99)00093-0.

Knox, S. H., C. Sturtevant, J. H. Matthes, L. Koteen, J. Verfaillie, and D. Baldocchi (2015), Agricultural peatland restoration: Effects of land-use change on greenhouse gas (CO_2 and CH_4) fluxes in the Sacramento-San Joaquin Delta, *Global Change Biol.*, *21*(2), 750–765, doi:10.1111/gcb.12745.

Koebsch, F., G. Jurasinski, M. Koch, J. Hofmann, and S. Glatzel (2015), Controls for multi-scale temporal variation in ecosystem methane exchange during the growing season of a permanently inundated fen, *Agric. For. Meteorol.*, *204*, 94–105, doi:10.1016/j.agrformet.2015.02.002.

Kumar, P., and B. L. Ruddell (2010), Information driven ecohydrologic self-organization, *Entropy*, *12*(10), 2085–2096, doi:10.3390/e12102085.

Kumar, P., and E. Foufoula-Georgiou (1997), Wavelet analysis for geophysical applications, *Rev. Geophys.*, *35*(4), 385–412, doi:10.1029/97RG00427.

Long, K. D., L. B. Flanagan, and T. Cai (2010), Diurnal and seasonal variation in methane emissions in a northern Canadian peatland measured by eddy covariance, *Global Change Biol.*, *16*(9), 2420–2435, doi:10.1111/j.1365-2486.2009.02083.x.

Mack, S. K., R. R. Lane, and J. W. Day (2012), The restoration of degraded deltaic wetlands of the Mississippi Delta *Rep.*, American Carbon Registry, Tierra Resources.

Mallat, S. G. (1989), A theory for multiresolution signal decomposition: The wavelet representation, *IEEE Trans. Pattern Anal. Mach. Intell.*, *11*(7), 674–693, doi:10.1109/34.192463.

Matthes, J. H., C. Sturtevant, J. Verfaillie, S. Knox, and D. Baldocchi (2014), Parsing the variability in CH_4 flux at a spatially heterogeneous wetland: Integrating multiple eddy covariance towers with high-resolution flux footprint analysis, *J. Geophys. Res. Biogeosci.*, *119*, 1322–1339, doi:10.1002/2014JG002642.

Miller, R. L. (2011), Carbon gas fluxes in re-established wetlands on organic soils differ relative to plant community and hydrology, *Wetlands*, *31*(6), 1055–1066, doi:10.1007/s13157-011-0215-2.

Minoda, T., and M. Kimura (1994), Contribution of photosynthesized carbon to the methane emitted from paddy fields, *Geophys. Res. Lett.*, *21*(18), 2007–2010, doi:10.1029/94GL01595.

Molini, A., G. G. Katul, and A. Porporato (2010), Causality across rainfall time scales revealed by continuous wavelet transforms, *J. Geophys. Res.*, *115*, D14123, doi:10.1029/2009JD013016.
Moore, T. R., and M. Dalva (1993), The influence of temperature and water-table position on carbon-dioxide and methane emissions from laboratory columns of peatland soils, *J. Soil Sci.*, *44*(4), 651–664.
Morin, T. H., G. Bohrer, L. Naor-Azrieli, S. Mesi, W. T. Kenny, W. J. Mitsch, and K. V. R. Schafer (2014), The seasonal and diurnal dynamics of methane flux at a created urban wetland, *Ecol. Eng.*, *72*, 74–83, doi:10.1016/j.ecoleng.2014.02.002.
Morrissey, L. A., D. B. Zobel, and G. P. Livingston (1993), Significance of stomatal control on methane release from carex-dominated wetlands, *Chemosphere*, *26*(1–4), 339–355, doi:10.1016/0045-6535(93)90430-d.
Paluš, M. (2008), From nonlinearity to causality: Statistical testing and inference of physical mechanisms underlying complex dynamics, *Contemp. Phys.*, *48*(6), 307–348, doi:10.1080/00107510801959206.
Parrott, L. (2010), Measuring ecological complexity, *Ecol. Indic.*, *10*(6), 1069–1076, doi:10.1016/j.ecolind.2010.03.014.
Percival, D. B., and A. T. Walden (2000), *Wavelet Methods for Time Series Analysis*, Cambridge Univ. Press, Cambridge, U. K.
Percival, D. P. (1995), On estimation of the wavelet variance, *Biometrika*, *82*(3), 619–631, doi:10.1093/biomet/82.3.619.
Qin, Z., Y. Ouyang, G. L. Su, Q. Yu, J. Li, J. E. Zhang, and Z. Y. Wu (2008), Characterization of CO_2 and water vapor fluxes in a summer maize field with wavelet analysis, *Ecol. Inform.*, *3*(6), 397–409, doi:10.1016/j.ecoinf.2008.09.002.
Reid, M. C., R. Tripathee, K. V. R. Schafer, and P. R. Jaffe (2013), Tidal marsh methane dynamics: Difference in seasonal lags in emissions driven by storage in vegetated versus unvegetated sediments, *J. Geophys. Res.-Biogeosci.*, *118*, 1802–1813, doi:10.1002/2013JG002438.
Richardson, A. D., D. Y. Hollinger, J. D. Aber, S. V. Ollinger, and B. H. Braswell (2007), Environmental variation is directly responsible for short- but not long-term variation in forest-atmosphere carbon exchange, *Global Change Biol.*, *13*(4), 788–803, doi:10.1111/j.1365-2486.2007.01330.x.
Ruddell, B. L., and P. Kumar (2009a), Ecohydrologic process networks: 2. Analysis and characterization, *Water Resour. Res.*, *45*, W03420, doi:10.1029/2008WR007280.
Ruddell, B. L., and P. Kumar (2009b), Ecohydrologic process networks: 1. Identification, *Water Resour. Res.*, *45*, W03419, doi:10.1029/2008WR007279.
Ruddell, B. L., C. Sturtevant, M. Kang, and R. Yu (2008), ProcessNetwork Software, version 1.5. [Available at http://www.mathworks.com/matlabcentral/fileexchange/41515-processnetwork-version-1-5-software], on October 4, 2015.
Ruddell, B., R. Yu, M. Kang, and D. Childers (2015), Seasonally varied controls of climate and phenophase on terrestrial carbon dynamics: modeling eco-climate system state using Dynamical Process Networks, *Landsc. Ecol.*, 1–16, doi:10.1007/s10980-015-0253-x.
Sachs, T., C. Wille, J. Boike, and L. Kutzbach (2008), Environmental controls on ecosystem-scale CH_4 emission from polygonal tundra in the Lena River Delta, Siberia, *J. Geophys. Res.*, *113*, G00A03, doi:10.1029/2007JG000505.
Schreiber, T. (2000), Measuring information transfer, *Phys. Rev. Lett.*, *85*(2), 461–464.
Shannon, C. E. (1948), A mathematical theory of communication, part 1, *Bell Syst. Tech. J.*, *27*, 379–423.
Sharma, A., and R. Mehrotra (2014), An information theoretic alternative to model a natural system using observational information alone, *Water Resour. Res.*, *50*, 650–660, doi:10.1002/2013WR013845.
Song, C., L. Sun, Y. Huang, Y. Wang, and Z. Wan (2011), Carbon exchange in a freshwater marsh in the Sanjiang Plain, northeastern China, *Agric. For. Meteorol.*, *151*(8), 1131–1138, doi:10.1016/j.agrformet.2011.04.001.
Sorrell, B. K., and H. Brix (2003), Effects of water vapour pressure deficit and stomatal conductance on photosynthesis, internal pressurization and convective flow in three emergent wetland plants, *Plant Soil*, *253*(1), 71–79, doi:10.1023/a:1024517510541.
Stengel, E. (1993), Species-specific aeration of water by different vegetation types in constructed wetlands, in *Constructed Wetlands for Water Quality Improvement*, edited by G. A. Moshiri, pp. 427–434, Lewis Publishers Inc., Boca Raton, Fla.
Stoy, P. C., G. G. Katul, M. B. S. Siqueira, J.-Y. Juang, H. R. McCarthy, H.-S. Kim, A. C. Oishi, and R. Oren (2005), Variability in net ecosystem exchange from hourly to inter-annual time scales at adjacent pine and hardwood forests: A wavelet analysis, *Tree Physiol.*, *25*(7), 887–902, doi:10.1093/treephys/25.7.887.
Stoy, P. C., M. Williams, M. Disney, A. Prieto-Blanco, B. Huntley, R. Baxter, and P. Lewis (2009a), Upscaling as ecological information transfer: A simple framework with application to Arctic ecosystem carbon exchange, *Landsc. Ecol.*, *24*(7), 971–986, doi:10.1007/s10980-009-9367-3.
Stoy, P. C., M. Williams, L. Spadavecchia, R. A. Bell, A. Prieto-Blanco, J. G. Evans, and M. T. van Wijk (2009b), Using information theory to determine optimum pixel size and shape for ecological studies: Aggregating land surface characteristics in arctic ecosystems, *Ecosystems*, *12*(4), 574–589, doi:10.1007/s10021-009-9243-7.
Strachan, I. B., K. A. Nugent, S. Crombie, and M.-C. Bonneville (2015), Carbon dioxide and methane exchange at a cool-temperate freshwater marsh, *Environ. Res. Lett.*, *10*(6), 065006, doi:10.1088/1748-9326/10/6/065006.
Sun, L., C. Song, Y. Miao, T. Qiao, and C. Gong (2013), Temporal and spatial variability of methane emissions in a northern temperate marsh, *Atmos. Environ.*, *81*, 356–363, doi:10.1016/j.atmosenv.2013.09.033.
Torrence, C., and G. P. Compo (1998), A practical guide to wavelet analysis, *Bull. Am. Meteorol. Soc.*, *79*(1), 61–78, doi:10.1175/1520-0477(1998)079<0061:apgtwa>2.0.co;2.
Turetsky, M. R., et al. (2014), A synthesis of methane emissions from 71 northern, temperate, and subtropical wetlands, *Global Change Biol.*, 2183–2197, doi:10.1111/gcb.12580.
Updegraff, K., S. D. Bridgham, J. Pastor, P. Weishampel, and C. Harth (2001), Response of CO_2 and CH_4 emissions from peatlands to warming and water table manipulation, *Ecol. Appl.*, *11*(2), 311–326.
Van der Nat, F., J. J. Middelburg, D. Van Meteren, and A. Wielemakers (1998), Diel methane emission patterns from Scirpus lacustris and Phragmites australis, *Biogeochemistry*, *41*(1), 1–22, doi:10.1023/a:1005933100905.
Wassmann, R., H. U. Neue, R. S. Lantin, K. Makarim, N. Chareonsilp, L. V. Buendia, and H. Rennenberg (2000), Characterization of methane emissions from rice fields in Asia. II Differences among irrigated, rainfed, and deepwater rice, *Nutr. Cycling Agroecosyst.*, *58*(1–3), 13–22, doi:10.1023/a:1009822030832.
Whiting, G. J., and J. P. Chanton (1993), Primary production control of methane emission from wetlands, *Nature*, *364*(6440), 794–795.
Whiting, G. J., and J. P. Chanton (1996), Control of the diurnal pattern of methane emission from emergent aquatic macrophytes by gas transport mechanisms, *Aquat. Bot.*, *54*(2–3), 237–253, doi:10.1016/0304-3770(96)01048-0.
Wille, C., L. Kutzbach, T. Sachs, D. Wagner, and E. M. Pfeiffer (2008), Methane emission from Siberian arctic polygonal tundra: Eddy covariance measurements and modeling, *Global Change Biol.*, *14*(6), 1395–1408, doi:10.1111/j.1365-2486.2008.01586.x.
Windsor, J., T. R. Moore, and N. T. Roulet (1992), Episodic fluxes of methane from sub-arctic fens, *Can. J. Soil Sci.*, *72*(4), 441–452.
Yagi, K., H. Tsuruta, K.-i. Kanda, and K. Minami (1996), Effect of water management on methane emission from a Japanese rice paddy field: Automated methane monitoring, *Global Biogeochem. Cycles*, *10*(2), 255–267, doi:10.1029/96GB00517.
Yoshida, M., T. Ohta, A. Kotani, and T. Maximov (2010), Environmental factors controlling forest evapotranspiration and surface conductance on a multi-temporal scale in growing seasons of a Siberian larch forest, *J. Hydrol.*, *395*(3–4), 180–189, doi:10.1016/j.jhydrol.2010.10.023.